

LETTERS • OPEN ACCESS

Thermal power generation during heat cycle near room temperature

To cite this article: Takayuki Shibata *et al* 2018 *Appl. Phys. Express* **11** 017101

View the [article online](#) for updates and enhancements.

Related content

- [Cobalt Hexacyanoferrate as Cathode Material for Na⁺ Secondary Battery](#)
Masamitsu Takachi, Tomoyuki Matsuda and Yutaka Moritomo
- [Concentration dependence of Li⁺/Na⁺ diffusion in manganese hexacyanoferrates](#)
Masamitsu Takachi, Yuya Fukuzumi and Yutaka Moritomo
- [Redox Reactions in Prussian Blue Analogue Films with Fast Na⁺ Intercalation](#)
Masamitsu Takachi, Tomoyuki Matsuda and Yutaka Moritomo



Thermal power generation during heat cycle near room temperature

Takayuki Shibata¹, Yuya Fukuzumi², Wataru Kobayashi^{2,3,4}, and Yutaka Moritomo^{2,3,4*}

¹National Institute of Technology, Gunma College, Maebashi 371-8530, Japan

²Graduate School of Pure and Applied Science, University of Tsukuba, Tsukuba, Ibaraki 305-8571, Japan

³Faculty of Pure and Applied Science, University of Tsukuba, Tsukuba, Ibaraki 305-8571, Japan

⁴Tsukuba Research Center for Energy Materials Science (TREMS), University of Tsukuba, Tsukuba, Ibaraki 305-8571, Japan

*E-mail: moritomo.yuktaka.gf@u.tsukuba.ac.jp

Received September 15, 2017; accepted November 17, 2017; published online December 8, 2017

We demonstrate that a sodium-ion secondary battery (SIB)-type thermocell consisting of two types of Prussian blue analogue (PBA) with different electrochemical thermoelectric coefficients ($S_{EC} \equiv \partial V / \partial T$; V and T are the redox potential and temperature, respectively) produces electrical energy during heat cycles. The device produces an electrical energy of 2.3 meV/PBA per heat cycle between 295 K ($= T_L$) and 323 K ($= T_H$). The ideal thermal efficiency ($\eta = 1.0\%$), which is evaluated using the heat capacity ($C = 4.16$ meV/K) of ideal $\text{Na}_2\text{Co}[\text{Fe}(\text{CN})_6]$, reaches 11% of the Carnot efficiency ($\eta_{th} = 8.7\%$). Our SIB-type thermocell is a promising thermoelectric device that harvests waste heat near room temperature.

© 2018 The Japan Society of Applied Physics

The thermoelectric device, which can convert heat into electricity and vice versa, is a fascinating technology for a smart society. In the development of thermoelectric semiconductors, the Seebeck coefficient [$S \equiv \Delta V / \Delta T$, where ΔV (ΔT) is the voltage (temperature) difference between the hot and cold electrodes] is a significant material parameter. Bi_2Te_3 ($S = 0.2$ mV/K¹ at room temperature) and PbTe ($= 0.12$ mV/K² at 300 K) are prototypical semiconductors and exhibit high dimensionless figures of merit ($ZT \equiv S^2 / \rho \kappa T$, where T , ρ , and κ represent the temperature, resistivity, and thermal conductivity, respectively). Moreover, they have practical use for Peltier cooling and power generation in space vehicles.³⁾ These devices, however, require a high-grade heat source of several hundred Kelvins to achieve a thermal efficiency of $\sim 10\%$.⁴⁾

On the other hand, several thermocells, which consist of hot and cold electrodes of identical type and solvable redox couples, were proposed in the 1950s and 1960s. The thermocell converts ΔT into ΔV between the electrodes through the electrochemical thermoelectric coefficient ($S_{EC} \equiv \partial V / \partial T$, where V and T are the redox potential and temperature, respectively). For example, a thermocell using $[\text{Fe}(\text{CN})_6]^{3+} / [\text{Fe}(\text{CN})_6]^{4+}$ ⁵⁾ was demonstrated to convert ΔT into ΔV between the two electrodes. The thermocell, however, needs a pump to transfer the accumulated species from the electrode region, which results in the loss of a major advantage, the absence of moving parts. Kobayashi et al.⁶⁾ proposed a sodium-ion secondary battery (SIB)-type thermocell, whose configuration is the same as that of a SIB, except that the anode and cathode materials are the same. They fabricated a CR2032-type thermocell made of layered oxides, for example, $\text{Na}_{0.99}\text{CoO}_2$ and $\text{Na}_{0.52}\text{MnO}_2$, and confirmed that ΔV changes linearly with ΔT . Compared to the aforementioned thermocell, the SIB-type thermocell utilizes the S_{EC} value of a redoxable solid, and hence has no moving parts.

If the thermocell is made of two types of redox material with different S_{EC} , the heating/cooling of the thermocell changes the cell voltage (V_{cell}) between the anode and cathode. In other words, such a thermocell produces electrical energy during heat cycles, in sharp contrast with the thermoelectric devices described above. Lee et al.⁷⁾ and Yang et al.⁸⁾ demon-

strated that this idea is feasible using solvable redox couples,⁹⁾ for example, $[\text{Fe}(\text{CN})_6]^{3+} / [\text{Fe}(\text{CN})_6]^{4+}$ and $\text{Cu}^+ / \text{Cu}^{2+}$, as the anode and Prussian blue analogues (PBAs) as the cathode. These thermocells, however, are bulky and heavy because the electrolyte contains redoxable ions. To overcome this drawback, we propose a SIB-type thermocell that consists of two types of redoxable solid with different S_{EC} . It is possible to minimize the amount of electrolyte used in this thermocell. This type of thermocell extends the use of so-called battery materials from energy storage to energy conversion.

PBAs, whose chemical formulas are $\text{Li}_x\text{M}[\text{Fe}(\text{CN})_6]_y$ and $\text{Na}_x\text{M}[\text{Fe}(\text{CN})_6]_y$ (where M is a transition metal), are promising candidates for use as the cathode materials in lithium ion batteries and SIBs.^{10–21)} For example, a thin film of $\text{Li}_{1.6}\text{Co}[\text{Fe}(\text{CN})_6]_{0.9}2.9\text{H}_2\text{O}$ shows a high capacity of 132 mAh/g with good cyclability.¹²⁾ PBAs have face-centered cubic structure ($Fm\bar{3}m$; $Z = 4$). They consist of a three-dimensional (3D) jungle-gym-type host framework and guest Li^+ ions, which are accommodated in the nanopores of the framework. Importantly, the host framework, $\text{Fe}-\text{CN}-M-\text{NC}-\text{Fe}$, is robust against $\text{Li}^+ / \text{Na}^+$ deintercalation and concomitant oxidization of M and Fe . In fact, the host framework of $\text{Li}_{1.6}\text{Co}[\text{Fe}(\text{CN})_6]_{0.9}2.9\text{H}_2\text{O}$ is stable even if we remove all of the Li^+ from the framework.¹²⁾ Recently, Magnússon et al.²²⁾ systematically investigated the S_{EC} ²³⁾ value of $\text{Li}_x\text{Co}[\text{Fe}(\text{CN})_6]_y$ for various x and y .

In this study, we fabricated a SIB-type thermocell with a thin film of $\text{Na}_x\text{Co}[\text{Fe}(\text{CN})_6]_{0.71}3.6\text{H}_2\text{O}$ (NCF71) as the anode and a thin film of $\text{Na}_x\text{Co}[\text{Fe}(\text{CN})_6]_{0.9}2.9\text{H}_2\text{O}$ (NCF90) as the cathode. The S_{EC} values are 0.53 and 1.32 mV/K for NCF71 at $x = 0.51$ and NCF90 at $x = 0.71$, respectively. Owing to the difference in S_{EC} , the device produces an electrical energy of 2.3 meV/NCF90 per heat cycle between 295 K ($= T_L$) and 323 K ($= T_H$). The ideal thermal efficiency ($\eta = 1.0\%$) reaches 11% of the Carnot efficiency ($\eta_{th} \equiv 1 - T_L / T_H = 8.7\%$).

The NCF71 and NCF90 films were synthesized by means of electrochemical deposition on indium tin oxide transparent electrodes. Details of the synthesis conditions are described in the literature.^{24,25)} The chemical compositions of the films were determined by the inductively coupled plasma method



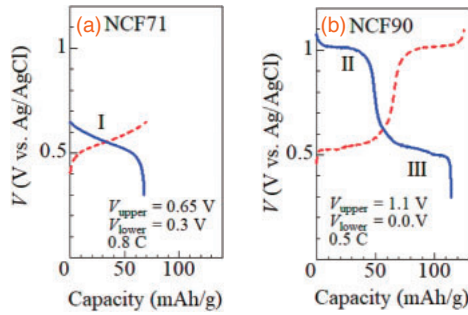


Fig. 1. Charge (red broken curve) and discharge (blue solid curve) curves of (a) $\text{Na}_x\text{Co}[\text{Fe}(\text{CN})_6]_{0.71}$ (NCF71) and (b) $\text{Na}_x\text{Co}[\text{Fe}(\text{CN})_6]_{0.9}$ (NCF90) films measured in aqueous solution of 10 mol/L NaClO_4 . For convenience of explanation, we defined plateaus I, II, and III in the discharge curves. V_{upper} and V_{lower} are the upper and lower cutoff voltages, respectively.

and CHN organic elementary analysis (PerkinElmer 2400 CHN Elemental Analyzer). Both the compounds show face-centered cubic structure ($Fm\bar{3}m$; $Z = 4$) with lattice constants (a) of 10.3 Å (NCF71) and 10.4 Å (NCF90). The film thickness is $\approx 1.0 \mu\text{m}$, as determined by a profilometer (Ulvac DEKTAK3030). The typical area of a film is 1.0 cm^2 . The mass of each film was evaluated from the thickness, area, and ideal density.

Figures 1(a) and 1(b) show the charge and discharge curves of the NCF71 and NCF90 films, respectively, in an aqueous solution of 10 mol/L NaClO_4 . The electrochemical properties of the films were investigated using a potentiostat (HOKUTO DENKO HJ1001SD8) with a beaker-type cell in the three-pole configuration. The working, reference, and counter electrodes were the PBA films, a standard Ag/AgCl electrode, and Pt, respectively. In NCF71 [Fig. 1(a)], the discharge curve shows a single plateau (plateau I) at $\approx 0.55 \text{ V}$ versus Ag/AgCl, which is ascribed to the reduction reaction²⁴⁾ $\text{Na}_{0.13}\text{Co}^{2+}[\text{Fe}_{0.71}^{3+}\text{Fe}_{0.29}^{2+}(\text{CN})_6]_{0.71} + 0.71\text{Na}^+ \rightarrow \text{Na}_{0.84}\text{Co}^{2+}[\text{Fe}^{2+}(\text{CN})_6]_{0.71}$. The discharge capacity is 68 mAh/g, which is close to the ideal value ($= 72 \text{ mAh/g}$). In the discharge process, Na^+ is inserted into the framework, which causes the reduction of Fe^{3+} to maintain charge neutrality. In NCF90 [Fig. 1(b)], the discharge curve shows two plateaus (plateaus II and III) at ≈ 1.0 and $\approx 0.53 \text{ V}$. Plateau II ($x \leq 0.6$) at $\approx 1.0 \text{ V}$ is ascribed to the reaction¹⁶⁾ $\text{Co}^{3+}[\text{Fe}_{0.6}^{3+}\text{Fe}_{0.4}^{2+}(\text{CN})_6]_{0.9} + 0.6\text{Na}^+ \rightarrow \text{Na}_{0.6}\text{Co}^{3+}[\text{Fe}^{2+}(\text{CN})_6]_{0.9}$. Plateau III ($x \geq 0.6$) at $\approx 0.53 \text{ V}$ is ascribed to the reaction^{16,25)} $\text{Na}_{0.6}\text{Co}^{3+}[\text{Fe}^{2+}(\text{CN})_6]_{0.9} + \text{Na}^+ \rightarrow \text{Na}_{1.6}\text{Co}^{2+}[\text{Fe}^{2+}(\text{CN})_6]_{0.9}$. The discharge capacity is 115 mAh/g, which is close to the ideal value ($= 132 \text{ mAh/g}$). We use plateau I of the NCF71 film and plateau III of the NCF90 film in the SIB-type thermocell because their redox potentials are almost the same.

To determine the S_{EC} values of the NCF71 (plateau I) and NCF90 (plateau III; $x \geq 0.6$) films, we fabricated a specially designed two-pole cell whose anode (T_{anode}) and cathode (T_{cathode}) temperatures are independently controlled by Peltier elements. The cathode, anode, and electrolyte were the thin film, Na metal, and propylene carbonate containing 1 mol/L NaClO_4 , respectively. We carefully measured V against T_{cathode} with T_{anode} fixed at 295.3 K. Figures 2(a) and 2(b) show the V values of NCF71 at $x = 0.51$ at plateau I and of NCF90 at $x = 0.71$ at plateau III, respectively, against T_{cathode} . We evaluated S_{EC} by least-squares fittings with primary functions, as indicated by the solid straight lines.

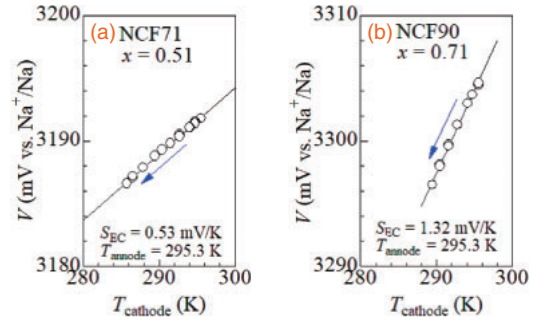


Fig. 2. Redox potential (V) of (a) NCF71 at $x = 0.51$ and (b) NCF90 at $x = 0.71$ against temperature (T_{cathode}) of cathode. Temperature (T_{anode}) of anode was fixed at 295.3 K. x in NCF71 (NCF90) was evaluated from the moved charge under the assumption that $x = 0.84$ (1.6) in the discharged state and 0.13 (0.0) in the charged state. Solid straight lines are results of least-squares fitting.

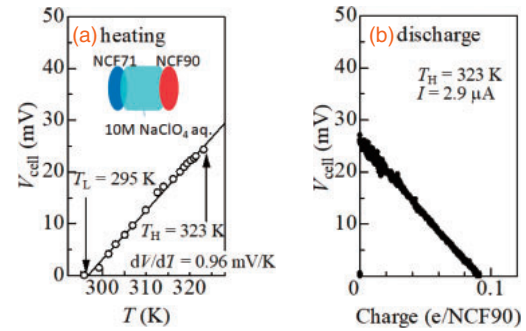


Fig. 3. (a) V_{cell} of the SIB-type thermocell against T . T_{L} ($= 295 \text{ K}$) and T_{H} ($= 323 \text{ K}$) are the lowest and highest temperatures, respectively. Inset shows schematic picture of the thermocell. (b) First discharge process at T_{H} under a constant current condition ($I = 2.9 \mu\text{A}$). The moved charge was normalized by that of NCF90.

Thus, the S_{EC} values are determined to be 0.53 and 1.32 mV/K for NCF71 at $x = 0.51$ (plateau I) and NCF90 at $x = 0.71$ (plateau III), respectively. The difference ($= 0.79 \text{ mV/K}$) in S_{EC} between NCF71 and NCF90 is significant.

We fabricate a SIB-type thermocell (two-pole beaker-type cell) whose anode, cathode and electrolyte are the as-grown NCF71 film, a pre-oxidized NCF90 film, and an aqueous solution of 10 mol/L NaClO_4 , respectively (inset of Fig. 3). The NCF90 film was pre-oxidized at $V_{\text{upper}} = 0.65 \text{ V}$ against Ag/AgCl in an aqueous solution of 10 mol/L NaClO_4 . Here, we defined T_{L} ($= 295 \text{ K}$) and T_{H} ($= 323 \text{ K}$) as the lowest and highest temperatures, respectively. The as-prepared device, which showed a finite V_{cell} ($= 0.19 \text{ V}$), was discharged to 0 V under a constant current condition ($I = 7.3 \mu\text{A}$). Then, we slowly increased the temperature (T) of the device from T_{L} to T_{H} . Figure 3(a) shows V_{cell} against T in this heating process. As expected, V_{cell} increases linearly with T at a rate of 0.96 mV/K. The increase in V_{cell} is reasonably ascribed to the difference in S_{EC} between the anode and cathode. Moreover, the observed value ($= 0.96 \text{ mV}$) is close to the difference ($= 0.79 \text{ mV}$) in S_{EC} between NCF71 and NCF90. At T_{H} , the device shows a finite V_{cell} ($= 26 \text{ mV}$). Figure 3(b) shows the first discharge process at T_{H} at $I = 2.9 \mu\text{A}$. V_{cell} decreases linearly to 0 V in proportion to the moved charge. The final moved charge is 0.09 e per NCF90 unit. The electric work done in this discharge process was 1.2 meV/NCF90.

The heat cycle of the SIB-type thermocell consists of four processes, as shown schematically in Fig. 4: (i) heating from

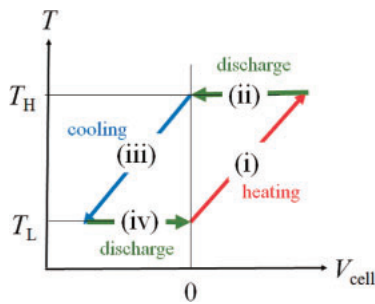


Fig. 4. Heat cycle of SIB-type thermocell against V_{cell} and T . The heat cycle consists of four processes: (i) heating from T_L to T_H , (ii) discharge at T_H , (iii) cooling from T_H to T_L , and (iv) discharge at T_L . The heating and cooling processes are performed without current ($I = 0$).

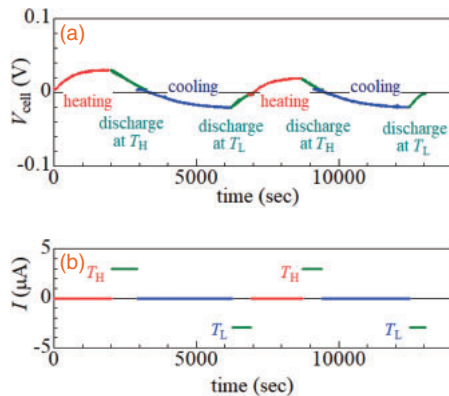


Fig. 5. (a) V_{cell} and (b) I in the SIB-type thermocell against time in the first and second heat cycles. The lowest (T_L) and highest (T_H) temperatures are 295 and 323 K, respectively. The discharge processes were performed under a constant current condition ($I = 2.9 \mu\text{A}$).

T_L to T_H , (ii) discharge at T_H , (iii) cooling from T_H to T_L , and (iv) discharge at T_L . Figures 5(a) and 5(b) show the variation in V_{cell} and current (I), respectively, during the first and second heat cycles. In the heating process [(i)], V_{cell} gradually increases with time and eventually reaches $V_{\text{cell}} = 26 \text{ mV}$ at T_H . The discharge process [(ii)] at T_H produces an electrical energy of 1.2 meV/NCF90 under a constant current condition ($I = 2.9 \mu\text{A}$). In the cooling process [(iii)], V_{cell} gradually decreases with time and eventually reaches $V_{\text{cell}} = -25 \text{ mV}$ at T_L . Like process (ii), the discharge process [(iv)] at T_L produces electrical energy. Note that the signs of both the current and the voltage are opposite for processes (ii) and (iv).

Now, let us discuss the thermal efficiency ($\eta \equiv W/Q$, where W and Q are the output work and input thermal energy, respectively) of the SIB-type thermocell. The output work (W) is expressed as $W = W_H + W_L$, where W_H and W_L are the electrical work during the discharge processes at T_L and T_H . $W = 2W_H (= 2.3 \text{ meV/NCF90})$, because W_L is essentially the same as W_H . The input thermal energy is $C_{\text{tot}}(T_H - T_L)$, where C_{tot} is the sum of the specific heats of the anode (C_{anode}) and cathode (C_{cathode}). Here, let us use the calculated $C_{\text{PBA}} (= 4.16 \text{ meV/K})$ of ideal $\text{Na}_2\text{Co}[\text{Fe}(\text{CN})_6]$ in the Dulong–Petit law. Then, $Q (= 233 \text{ meV})$ is easily evaluated considering $C_{\text{tot}} = C_{\text{anode}} + C_{\text{cathode}} = 2C_{\text{PBA}}$. Thus, we obtained $\eta = 1.0\%$. Strictly speaking, we should include the heat capacity of the electrolyte in the thermal efficiency. The amount of electrolyte, however, is minimized in the SIB-type thermocell because the thermocell utilizes redoxable solids.

In this sense, $\eta (= 1.0\%)$ is an ideal value. Incidentally, the Carnot efficiency ($\eta_{\text{th}} \equiv 1 - T_L/T_H$) is 8.7% between $T_L (= 295 \text{ K})$ and $T_H (= 323 \text{ K})$. Thus, the experimentally obtained $\eta (= 1.0\%)$ is 11% of the ideal value ($\eta_{\text{th}} = 8.7\%$). We will bring η closer to η_{th} by further development of anode and cathode materials with high $|S_{\text{EC}}|$ and flatter discharge curves. The flatter the discharge curve becomes, the more charge can be moved.

In conclusion, we demonstrate that a SIB-type thermocell consisting of two types of PBA with different S_{EC} values can harvest waste heat near room temperature. The device produces an electrical energy of 2.3 meV/NCF90 per heat cycle between 295 and 323 K. The ideal thermal efficiency ($\eta = 1.0\%$) reaches 11% of the Carnot efficiency ($\eta_{\text{th}} = 8.7\%$). We emphasize that our SIB-type thermocell can be easily formed into a sheet or a large device at a low cost, because it has the same device structure as SIBs.

Acknowledgments This work was supported by the Yazaki Memorial Foundation for Science and Technology and the Nippon Sheet Glass Foundation for Materials Science and Engineering. This work was also supported by JSPS KAKENHI (Grant Number JP17H0113). T.S. and W.K. were supported by the Nanotech Research Professional (NRP) course of the Nanotech Career-up Alliance in Nanotech (CUPAL) project. The elementary analyses were performed at the Chemical Analysis Division, Research Facility Center for Science and Engineering, University of Tsukuba.

- 1) D. A. Wright, *Nature* **181**, 834 (1958).
- 2) J. P. Heremans, V. Jovicic, E. S. Toberer, A. Saramat, K. Kurosaki, A. Charoenphakdee, S. Yamanaka, and G. J. Snyder, *Science* **321**, 554 (2008).
- 3) H. J. Goldsmid, *Introduction to Thermoelectricity* (Springer, Berlin, 2010).
- 4) C. B. Vining, *Nat. Mater.* **8**, 83 (2009).
- 5) T. Ikeshoji, *Bull. Chem. Soc. Jpn.* **60**, 1505 (1987).
- 6) W. Kobayashi, A. Kinoshita, and Y. Moritomo, *Appl. Phys. Lett.* **107**, 073906 (2015).
- 7) S. W. Lee, Y. Yang, H.-W. Lee, H. Ghasemi, D. Kraemer, G. Chen, and Y. Cui, *Nat. Commun.* **5**, 3942 (2014).
- 8) Y. Yang, S. W. Lee, H.-W. Lee, H. Ghasemi, J. Loomis, D. Kraemer, G. Zheng, Y. Cui, and G. Chen, *Proc. Natl. Acad. Sci. U.S.A.* **111**, 17011 (2014).
- 9) I. Quickenden and Y. Mua, *J. Electrochem. Soc.* **142**, 3985 (1995).
- 10) T. Matsuda and Y. Moritomo, *Appl. Phys. Express* **4**, 047101 (2011).
- 11) Y. Moritomo, M. Takachi, Y. Kurihara, and T. Matsuda, *Appl. Phys. Express* **5**, 041801 (2012).
- 12) M. Takachi, T. Matsuda, and Y. Moritomo, *Jpn. J. Appl. Phys.* **52**, 044301 (2013).
- 13) T. Matsuda, M. Takachi, and Y. Moritomo, *Chem. Commun.* **49**, 2750 (2013).
- 14) Y. Lu, L. Wang, J. Cheng, and J. B. Goodenough, *Chem. Commun.* **48**, 6544 (2012).
- 15) M. Takachi, T. Matsuda, and Y. Moritomo, *Appl. Phys. Express* **6**, 025802 (2013).
- 16) M. Takachi, T. Matsuda, and Y. Moritomo, *Jpn. J. Appl. Phys.* **52**, 090202 (2013).
- 17) D. Yang, J. Xu, X.-Z. Liao, Y.-S. He, H. Liu, and Z.-F. Ma, *Chem. Commun.* **50**, 13377 (2014).
- 18) H. W. Lee, R. Y. Wang, M. Pasta, S. W. Lee, N. Liu, and Y. Chi, *Nat. Commun.* **5**, 5280 (2014).
- 19) L. Wang, J. Song, R. Qiao, L. A. Wray, M. A. Hossain, Y. D. Chung, W. Yang, Y. Lu, D. Evans, J.-J. Lee, S. Vail, X. Ahaio, M. Nishijima, S. Kakimoto, and J. B. Torrance, *J. Am. Chem. Soc.* **137**, 2548 (2015).
- 20) S. Yu, Y. Li, Y. Lu, B. Xu, Q. Wang, M. Yan, and Y. A. Jing, *J. Power Sources* **275**, 45 (2015).
- 21) Y. You, X. L. Wu, Y. X. Yin, and Y. G. Guo, *Energy Environ. Sci.* **7**, 1643 (2014).
- 22) R. L. Magnússon, W. Kobayashi, M. Takachi, and Y. Moritomo, *AIP Adv.* **7**, 045002 (2017).
- 23) Note that the S_{EC} values reported in Ref. 22 is the difference between cathode (PBA) and anode (Li) material.
- 24) F. Nakada, H. Kamioka, Y. Moritomo, J. E. Kim, and M. Takata, *Phys. Rev. B* **77**, 224436 (2008).
- 25) K. Igarashi, F. Nakada, and Y. Moritomo, *Phys. Rev. B* **78**, 235106 (2008).